

# Single-crystal elasticity of phase Egg $\text{AlSi}_3\text{OH}$ and $\delta\text{-AlOOH}$ by Brillouin spectroscopy

BAOYUN WANG<sup>1,2,3</sup>, YANYAO ZHANG<sup>3</sup>, SUYU FU<sup>3,4</sup>, WEI YAN<sup>5,6</sup>, EIICHI TAKAHASHI<sup>1,7</sup>, LI LI<sup>1,7</sup>, JUNG-FU LIN<sup>3,\*</sup>, AND MAOSHUANG SONG<sup>1,7,\*</sup>

<sup>1</sup>State Key Laboratory of Isotope Geochemistry, Guangzhou Institute of Geochemistry, Chinese Academy of Sciences, Guangzhou 510640, China

<sup>2</sup>College of Earth and Planetary Sciences, University of Chinese Academy of Sciences, Beijing, 100049, China

<sup>3</sup>Department of Geological Sciences, Jackson School of Geosciences, The University of Texas at Austin, Austin, 78712 Texas, U.S.A.

<sup>4</sup>School of Earth and Space Exploration, Arizona State University, Tempe, Arizona 85287, U.S.A.

<sup>5</sup>School of Earth and Space Sciences, Peking University, Beijing 100871, China

<sup>6</sup>Key Laboratory of Orogenic Belts and Crustal Evolution, Ministry of Education of China, Beijing 100871, China

<sup>7</sup>CAS Center for Excellence in Deep Earth Science, Guangzhou 510640, China

## ABSTRACT

Phase Egg and  $\delta\text{-AlOOH}$  are two typical hydrous phases that might exist in the wet sedimentary layer of subducted slabs under mantle conditions. They are thus regarded as potential water carriers to Earth's deep mantle. In this report, we report the full elastic constants of both phases determined by Brillouin scattering and X-ray diffraction measurements under ambient conditions. Our results indicate that the hydrogen-bond configurations in the crystal structures of the two phases have a profound effect on their principal elastic constants. The adiabatic bulk modulus ( $K_S$ ) and shear modulus ( $G$ ) calculated from the obtained elastic constants using the Voigt-Reuss-Hill averaging scheme are 158.3(201) GPa and 123.0(60) GPa for phase Egg and 162.9(31) GPa and 145.2(13) GPa for  $\delta\text{-AlOOH}$ , respectively. These results allow us to evaluate elastic moduli and sound velocities of hydrous minerals in the  $\text{Al}_2\text{O}_3\text{-H}_2\text{O-SiO}_2$  ternary system (simplified composition of subducted wet sedimentary layer) at ambient conditions, including the contrast of the acoustic velocities  $V_p$  and  $V_s$  for the reaction  $\text{AlSi}_3\text{OH} = \delta\text{-AlOOH} + \text{SiO}_2$  (stishovite) and the evolution in the elastic moduli and sound velocities of hydrous minerals as a function of density.

**Keywords:** Phase Egg,  $\delta\text{-AlOOH}$ , elasticity, anisotropy, Brillouin spectroscopy

## INTRODUCTION

Hydrous phases that form in wet subducted lithospheric slabs are regarded as potential carriers for transporting water into the Earth's deep interior. Dehydration of these hydrous phases can release substantial amounts of water and significantly affect physical and chemical properties of the surrounding rocks, such as the rheology and electrical conductivity (Karato et al. 1986; Ohtani 2020). Researchers have examined phase relations in hydrous systems with various chemical compositions that are representative of sedimentary, basaltic and peridotitic layers of subducted slabs. These efforts have led to the discoveries of several hydrous minerals stable at relevant deep-mantle pressure-temperature conditions (Iwamori 2004; Litasov and Ohtani 2003; Schmidt and Poli 1998). Among these previously reported hydrous minerals in the simplified  $\text{Al}_2\text{O}_3\text{-H}_2\text{O-SiO}_2$  ternary system, phase Egg and  $\delta\text{-AlOOH}$  are two typical phases that might exist in the subducted wet sedimentary layer (Ono 1998; Schmidt et al. 1998). Experimental studies on the phase stability of phase Egg show that it remains stable at depths of the mantle transition zone even along a normal mantle geotherm. It then decomposes to  $\delta\text{-AlOOH}$  and stishovite at greater depths in the topmost lower mantle (25–30 GPa) (Fukuyama et al. 2017; Pamato et al. 2015; Sano et al. 2004).  $\delta\text{-AlOOH}$  is found to survive in the lower mantle down to core-mantle boundary conditions along a cold slab geotherm (Duan et al. 2018; Ohtani et al. 2001; Sano et al. 2008; Yuan et al. 2019). Therefore, phase Egg and  $\delta\text{-AlOOH}$

can form a continuous chain to transport water from the mantle transition zone to the deep lower mantle through slab subduction processes. In addition, Wirth et al. (2007) claimed that phase Egg occurs as inclusions in ultradeep diamonds, providing geological evidence for the possible existence of phase Egg at the depth of the mantle transition zone.

Phase Egg with an ideal formula of  $\text{AlSi}_3\text{OH}$  was first synthesized by Eggleton et al. (1978). It has a monoclinic symmetry with space group  $P2_1/n$  (Schmidt et al. 1998) and consists of edge-shared Si-octahedra linked to an  $\text{Al}_2\text{O}_{10}$  dimer (Online Materials<sup>1</sup> Fig. OM1a and OM1b). High-pressure X-ray diffraction studies show that the axial compressibility of phase Egg is extremely anisotropic (Schulze et al. 2018; Vanpeteghem et al. 2003), which is also supported by recent *first-principles* calculations (Mookherjee et al. 2019).  $\delta\text{-AlOOH}$  is a synthetic high-pressure polymorph of diasporite ( $\alpha\text{-AlOOH}$ ) and boehmite ( $\gamma\text{-AlOOH}$ ) that adopts a  $\text{CaCl}_2$ -type structure with  $P2_1nm$  space group (Online Materials<sup>1</sup> Fig. OM1c) (Suzuki et al. 2000). In recent years,  $\delta\text{-AlOOH}$  has drawn increasing attention due to its pressure-induced hydrogen-bond symmetrization and wide  $P\text{-}T$  stability field (Hsieh et al. 2020; Sano-Furukawa et al. 2018, 2009). The formation of  $\delta$ -phase  $\text{AlOOH-FeOOH-MgSiO}_3(\text{OH})_2$  solid solutions is of potential significance to deep-mantle water circulation and dynamic evolution (Yuan et al. 2019). Elastic data of phase Egg and  $\delta\text{-AlOOH}$  are basic physical parameters and essential for interpreting seismic observations and probing the possible existence of these phases in the Earth. Although *first-principles* calculations have been performed

\* E-mail: afu@jsg.utexas.edu and msong@gig.ac.cn

to explore the elastic properties of these two phases (Mookherjee et al. 2019; Tsuchiya and Tsuchiya 2009), few experimental studies have reported their elastic constants even under ambient conditions. To date, only one Brillouin scattering study has been performed on  $\delta\text{-AlOOH}$  polycrystalline aggregates (Mashino et al. 2016). Additionally, there are no available experimental elastic data for phase Egg with the exception of bulk modulus obtained from static compression X-ray diffraction experiments (Schulze et al. 2018; Vanpeteghem et al. 2003). Therefore, further experimental studies are required to shed new light on the elastic properties of these phases.

In this study, we performed Brillouin scattering and X-ray diffraction measurements on single-crystal phase Egg and  $\delta\text{-AlOOH}$  under ambient conditions. The full elastic tensors were extracted by fitting measured acoustic velocities as a function of the phonon directions using the Christoffel's equation (Every 1980). We quantified the adiabatic bulk moduli ( $K_S$ ), shear moduli ( $G$ ), compressional-wave velocities ( $V_P$ ), and shear-wave velocities ( $V_S$ ) of phase Egg and  $\delta\text{-AlOOH}$  under the Voigt-Reuss-Hill averaging scheme (Hill 1963). These results are compared with those of other typical hydrous minerals in the  $\text{Al}_2\text{O}_3\text{-SiO}_2\text{-H}_2\text{O}$  ternary system as a function of density to evaluate the correlation between these physical properties, compositions, and crystal structures.

## EXPERIMENTAL METHODS

### Synthesis and characterization of single crystals

High-quality single crystals of phase Egg and  $\delta\text{-AlOOH}$  were synthesized at high pressures and high temperatures using the Sakura 2500-ton multi-anvil apparatus at the Guangzhou Institute of Geochemistry, Chinese Academy of Sciences. To synthesize single-crystal phase Egg, a ground mixture of  $\text{CaO}$ ,  $\text{Al}(\text{OH})_3$ , and  $\text{SiO}_2$  in a 1:4:2 mole ratio was used as the starting material and sealed in a welded gold capsule. The synthesis experiment was conducted at 17 GPa and 1400 °C with a duration of 20 h (run no. U801). The recovered products were composed of single crystals of phase Egg with maximum dimensions of 200  $\mu\text{m}$  and some fine powders. The chemical compositions of several selected crystals were determined by electron microprobe analysis (EMPA) and are shown in Online Materials<sup>1</sup> Table OM1. Based on these analyses, the crystals have an average of 50.5(1) wt%  $\text{SiO}_2$  and 41.7(1) wt%  $\text{Al}_2\text{O}_3$ , yielding a chemical formula of  $\text{Al}_{0.98}\text{Si}_{1.01}\text{O}_4\text{H}_{1.02}$  with the H content estimated by the total weight deficiency. This formula is close to the composition of the ideal formula of phase Egg. The products were also characterized by single-crystal X-ray diffraction (XRD) and unpolarized FTIR measurements. The single-crystal XRD measurements were performed on a Bruker D8 Venture diffractometer equipped with a  $\text{MoK}\alpha$  radiation source (with a wavelength of 0.70926 Å), graphite monochromator,  $\omega$ -scanning, and Apex II CCD detector. These aforementioned characterizations confirm that the synthesized crystals are phase Egg. The crystal structure was further refined using the Olex2 package (Dolomanov et al. 2009), and the detailed atomic parameters are available as a CIF<sup>1</sup> file. Unpolarized FTIR spectra in the range of 600–7500  $\text{cm}^{-1}$  were recorded for several double-side polished crystals at ambient conditions using a Bruker Vertex 70 FTIR spectrometer combined with a Hyperion-2000 IR microscope and a HgCdTe (MCT) detector (Online Materials<sup>1</sup> Fig. OM2). The spectra show three evident absorption bands centered at ~2140, ~2434, and ~2784  $\text{cm}^{-1}$  (Online Materials<sup>1</sup> Fig. OM2), which could be assigned to be OH-stretching vibration of the phase Egg.

Single-crystal  $\delta\text{-AlOOH}$  was synthesized by following the procedure reported by Kawazoe et al. (2017). High-purity reagent-grade  $\text{Al}(\text{OH})_3$  powder (99.99%) was used as the starting material and the synthesis experiment was conducted at approximately 20 GPa and 1000 °C for a duration of 22 h (run no. U795). The recovered product is found to be composed of crystals with a maximum dimension of approximately 300  $\mu\text{m}$ . Analyses of synchrotron XRD patterns recorded at the 13-IDD beamline sector of GSECARS and EMPA measurements verify that the synthesized crystals are chemically homogeneous and pure  $\delta\text{-AlOOH}$  phase (Online Materials<sup>1</sup> Fig. OM3 and Table OM1).

### Sample preparation and Brillouin scattering measurements

To precisely constrain the 13 and 9 elastic constants of phase Egg (monoclinic,  $P2_1/n$ ) and  $\delta\text{-AlOOH}$  (orthorhombic,  $P2_1nm$ ), respectively, normally at least 3–4

platelets with different orientations are needed for Brillouin spectroscopic measurements. We carefully checked the synthesized crystals under a petrographic microscope and selected several high-quality clean and transparent crystals with homogeneous extinction for both phase Egg and  $\delta\text{-AlOOH}$ . With the selected single crystals of phase Egg, we prepared four double-side polished platelets with ~15  $\mu\text{m}$  thickness. To determine the crystallographic orientations and unit-cell parameters for these four platelets, single-crystal X-ray diffraction measurements were performed using an Agilent SuperNova diffractometer (Atlas S2 CCD detector,  $\text{MoK}\alpha$  radiation, graphite monochromator) in the  $\omega$ -scanning mode with the scanning step of 1° per frame. The scanning width varied from 80 to 100° and the exposure time varied from 7 to 15 s<sup>1</sup> depending on the crystals. The obtained X-ray diffraction images were analyzed using the CrysAlis Pro software (Oxford Diffraction 2006). The Miller indices of the polished platelets are determined to be (8, 3,  $\bar{5}$ ), (0,  $\bar{1}$ ,  $\bar{1}$ ), (45,  $\bar{6}$ , 13), and (2,  $\bar{1}$ , 2) with an estimated uncertainty less than 0.2. All four crystal platelets display very similar lattice parameters and unit-cell volumes, and the averaged values are  $a=7.1449(7)$  Å,  $b=4.3295(4)$  Å,  $c=6.9526(7)$  Å,  $\beta=98.35(9)^\circ$ , and  $V_0=201.79(4)$  Å<sup>3</sup>, which are consistent with values reported by previous studies (Schulze et al. 2018; Vanpeteghem et al. 2003). The derived density is 3.740(2)  $\text{g/cm}^3$  for phase Egg.

In the case of  $\delta\text{-AlOOH}$ , it was difficult to prepare single-crystal platelets with ideal crystallographic orientations as the synthesized crystals were often twin crystals. Fortunately, some crystals were large enough to allow us to collect Brillouin scattering signals from one single-crystal domain. Finally, we obtained three workable platelets for Brillouin scattering measurements. The orientations and lattice parameters of these platelets were determined by single-crystal XRD measurements at the 13-IDD beamline sector of GSECARS, Advanced Photon Source, Argonne National Laboratory. The incident X-ray beam has an energy of 37 keV and a focused beam size of 3–4  $\mu\text{m}$  at the sample. The geometry parameters were calibrated using the  $\text{LaB}_6$  standard. During XRD measurements, the wide-scan images of the single crystal platelets were collected from  $-15^\circ$  to  $+15^\circ$  with a total exposure time of 100 s. The obtained diffraction patterns were analyzed by GSE ADA/RSV software to derive crystallographic orientations (Dera et al. 2013). They were also integrated to one-dimensional profiles using Dioptas (Prescher and Prakapenka 2015). The Miller indices of the three platelets are determined to be (0, 0, 1), (2, 9, 2), and (10, 7, 3). The estimated accuracy of the measured Miller indices is within 0.1. The average lattice parameters of these three platelets are  $a=4.7093(8)$  Å,  $b=4.2271(1)$  Å,  $c=2.8302(1)$  Å, and  $V_0=56.34(5)$  Å<sup>3</sup>, with a calculated density of 3.536(1)  $\text{g/cm}^3$ .

Brillouin scattering measurements were conducted under ambient conditions using a Brillouin Light Scattering (BLS) system at the Mineral Physics Laboratory, the University of Texas at Austin (Fu et al. 2017, 2019; Zhang et al. 2021). In the BLS system, a single-frequency 532 nm solid-state green laser (Coherent Verdi V2) was used as an excitation light source and a JRS six-pass tandem Fabry–Pérot interferometer equipped with a Perkin–Elmer photomultiplier detector was used to record the Brillouin spectra of the sample. Samples were loaded into a short-symmetrical diamond-anvil cell without a pressure-transmitting medium. The laser beam was focused down to the sample with a spot size of approximately 20  $\mu\text{m}$  in diameter. In a symmetric forward scattering geometry, acoustic velocities ( $v$ ) were calculated from the measured Brillouin shifts ( $\Delta v$ ) through the equation (Whitfield et al. 1976):

$$v = \frac{\Delta v \cdot \lambda_0}{2 \sin(\theta/2)}$$

where  $\lambda_0$  is the laser wavelength of 532 nm,  $\theta$  is the external scattering angle of  $48.3(1)^\circ$  calibrated using water as a standard.

## RESULTS AND DISCUSSION

### Phase Egg

Brillouin scattering measurements were performed for each platelet of phase Egg in 19 distinct crystallographic directions by rotating the crystal in  $\chi$ -circle over an angular range of  $180^\circ$  with an interval of  $10^\circ$ . One typical Brillouin spectrum is shown in Figure 1a. In most cases, both the compressional acoustic mode ( $V_P$ ) and shear acoustic modes ( $V_{S1}$  and  $V_{S2}$ ) can be observed, but the  $V_P$  signal overlaps with the strong  $V_S$  peak of diamond in some directions where only  $V_{S1}$  and  $V_{S2}$  were observed. The dispersion of the measured acoustic velocities with the crystallographic directions for the four platelets of phase Egg are depicted in Figure 2. Together with the density from the single-crystal X-ray diffraction and EPMA compositional measurements, the measured

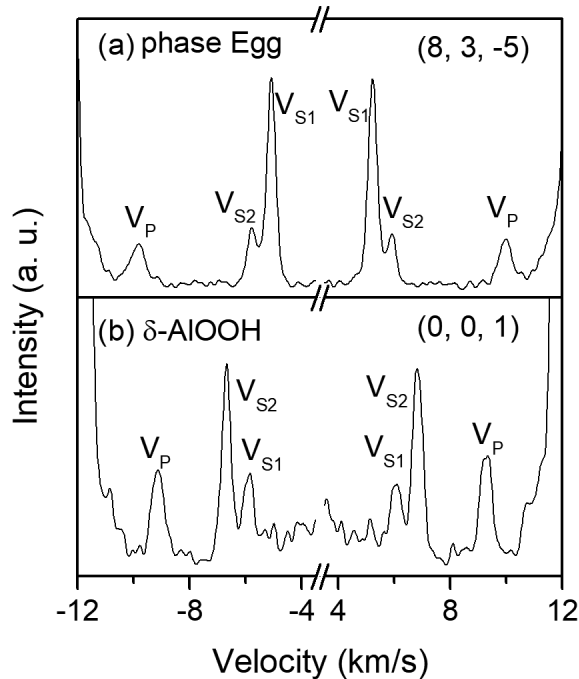


**FIGURE 1.** Representative Brillouin spectra of (a) phase Egg and (b)  $\delta$ -AIOOH at ambient conditions.  $V_p$ ,  $V_{S1}$ , and  $V_{S2}$  peaks are observed in both crystals. The Miller indices of each crystal platelet is shown at the top-right corner of the panel.

sound velocities are modeled to derive the 13 independent elastic constants of phase Egg by nonlinear least-squares fitting to Christoffel's equation (Every 1980). All the elastic constants  $C_{ij}$  based on the Cartesian coordinated system where the  $X$ -axis is parallel to the  $a^*$ -axis and  $Y$ -axis is parallel to the  $b$ -axis are given in Table 1 and compared with the theoretical values (Mookherjee et al.

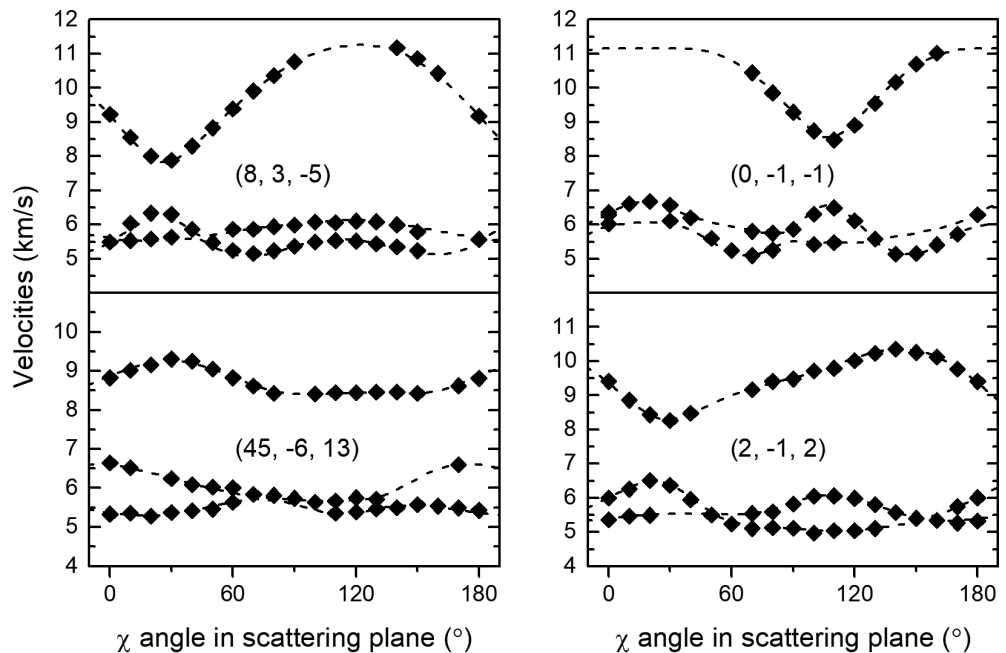
**TABLE 1.** Elastic properties of phase Egg and  $\delta$ -AIOOH under ambient conditions

	Phase Egg		$\delta$ -AIOOH		
	Experiment Single-crystal This study	Calculation - Mookherjee et al. (2019)	Experiment Single-crystal This study	Experiment Polycrystal Mashino et al. (2016)	
$\rho$ (g/cm <sup>3</sup> )	3.740(2)	3.798	3.536(1)		3.383
$C_{11}$ (GPa)	467.2(15)	504.7	375.9(9)		314
$C_{22}$ (GPa)	220.8(8)	280.4	295.4(11)		306
$C_{33}$ (GPa)	305.2(7)	401.0	433.5(12)		391
$C_{44}$ (GPa)	109.8(4)	150.3	129.2(6)		117
$C_{55}$ (GPa)	166.0(5)	174.0	133.4(7)		115
$C_{66}$ (GPa)	139.6(5)	159.7	166.4(6)		152
$C_{12}$ (GPa)	115.9(9)	98.6	49.7(9)		34
$C_{13}$ (GPa)	164.3(9)	141.6	91.9(15)		95
$C_{23}$ (GPa)	26.3(7)	87.9	52.8(21)		67
$C_{15}$ (GPa)	3.2(6)	7.5			
$C_{25}$ (GPa)	20.9(9)	13.5			
$C_{35}$ (GPa)	21.2(4)	19.8			
$C_{46}$ (GPa)	13.7(4)	18.6			
$K_{\text{Voigt}}$ (GPa)	178.5(8)	204.7	166.0(13)		155.9
$G_{\text{Voigt}}$ (GPa)	128.9(3)	154.0	146.5(3)		131.1
$K_{\text{Reuss}}$ (GPa)	138.2(46)	188.2	159.8(48)		151.2
$G_{\text{Reuss}}$ (GPa)	117.0(17)	148.4	144.0(15)		128.8
$K_{\text{VRH}}$ (GPa)	158.3(201)	196.4	162.9(31)		153.5
$G_{\text{VRH}}$ (GPa)	123.0(60)	151.2	145.2(13)		130.0
$V_p$ (km/s)	9.28(41)	10.25	10.04(7)	9.54(7)	9.83
$V_s$ (km/s)	5.73(14)	6.32	6.41(3)	5.89(10)	6.20

2019). Our values are systematically lower than the theoretical values of Mookherjee et al. (2019). Although the reason for this discrepancy is unclear, one possible reason is thermal effects due to their *first-principles* calculations being performed at  $T=0$  K (Mookherjee et al. 2019). Using the Voigt-Reuss-Hill averaging scheme (Hill 1963), aggregate properties such as  $K_S$ ,  $G$ ,  $V_p$ , and  $V_s$  are also calculated and given in Table 1.

The principal elastic constants of phase Egg exhibit the relationship  $C_{11} > C_{33} > C_{22}$ , while the shear elastic components display the order  $C_{55} > C_{66} > C_{44}$ . These relations can be well explained by

**FIGURE 2.** Measured velocities of single-crystal phase Egg as a function of  $\chi$  angle in the crystallographic plane. The Miller indices of the crystal platelets are shown in the panels. The dashed lines are calculated velocity dispersion curves using the fitted elastic constants of the crystal.



the orientation of the hydrogen bond, which is mostly aligned along the  $b$ -axis but tilted to have a component along the  $c$ -axis of the crystal structure. That is, the distortion of the SiO<sub>6</sub> octahedron with the longer Si-OH bond lies in the  $a$ - $c$  plane (Schmidt et al. 1998; Schulze et al. 2018) (Online Materials<sup>1</sup> Fig. OM1a and OM1b). The values of the principal elastic constants with  $C_{11}$  are twice as high as  $C_{22}$ , indicating that phase Egg has strikingly high anisotropy in the axial compressibility and that the  $b$ -axis is the most compressible direction. These observations are in agreement with previous static compression X-ray diffraction experiments (Schulze et al. 2018; Vanpeteghem et al. 2003).

The measured elastic constants of phase Egg allow us to evaluate the azimuthal anisotropy of the acoustic velocity. From 3D azimuthal images of the velocity distribution (Online Materials<sup>1</sup> Fig. OM4), we notice that the compressional-wave velocity varies from 7.68 to 11.34 km/s. The fastest compressional-wave velocity propagates along the direction that deviates  $\sim 38^\circ$  to the  $a$ -axis in the  $a$ - $c$  plane, and the slowest compressional-wave velocity propagates along the  $b$ -axis direction. Similarly, the shear-wave velocity also exhibits a strong directional dependence. The anisotropy factors of the compressional-wave and shear-wave velocities,  $AV = 200 \cdot (V_{\max} - V_{\min}) / (V_{\max} + V_{\min})$ , are calculated to be  $AV_p = 38.4\%$ ,  $AV_{S1} = 21.3\%$ , and  $AV_{S2} = 21.2\%$  (Online Materials<sup>1</sup> Figure OM4), and the shear-wave splitting factor, which is defined as  $AV_s = 200 \cdot (V_{S1} - V_{S2}) / (V_{S1} + V_{S2})$ , is calculated to be 22.1% (Online Materials<sup>1</sup> Fig. OM4).

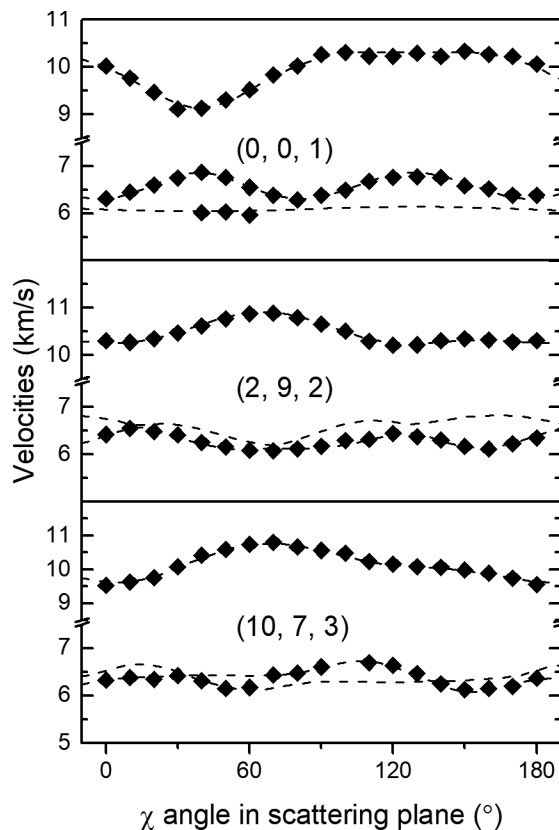


**FIGURE 3.** Measured velocities of single-crystal  $\delta$ -AIOOH as a function of  $\chi$  angle in the crystallographic plane. The Miller indices of the crystal platelets are shown in the panels. The dashed lines are calculated velocity dispersion curves using the fitted elastic constants.

## $\delta$ -AIOOH

Figure 1b shows a representative Brillouin spectrum of  $\delta$ -AIOOH. The measured acoustic velocities as a function of the crystallographic directions for the three  $\delta$ -AIOOH platelets are shown in Figure 3. The full nine independent elastic constants of  $\delta$ -AIOOH were inverted by fitting all the velocity data of the three platelets using Christoffel's equation, and the results are given in Table 1. Our values of the elastic constants are comparable with the theoretical values from *first-principles* simulations (Tsuchiya and Tsuchiya 2009). We found that the principal elastic constants exhibit the relation  $C_{33} > C_{11} > C_{22}$  and that  $C_{22}$  is much smaller than  $C_{33}$  and  $C_{11}$ . In accordance with this relation, the velocity along the  $c$ -axis is faster than those along the  $a$ -axis and  $b$ -axis by approximately 7.4% and 21.1%, respectively. The relation of  $C_{33} > C_{11} > C_{22}$  is also reflected in the strong elastic anisotropy in the axial compressibility for  $\delta$ -AIOOH, which is consistent with the fact that the O-H bond lies in the  $a$ - $b$  plane (see Online Materials<sup>1</sup> Figure OM1c). The compressibilities of the  $a$ - and the  $b$ -axes are higher than that of the  $c$ -axis. The anisotropic factors of  $\delta$ -AIOOH are calculated to be  $AV_p = 19.1\%$ ,  $AV_{S1} = 6.89\%$ , and  $AV_{S2} = 6.56\%$  (Online Materials<sup>1</sup> Fig. OM5). The shear-wave splitting factor is calculated to be  $AV_s = 12.65\%$  (Online Materials<sup>1</sup> Fig. OM5). The calculated isotropic aggregate properties of  $\delta$ -AIOOH are shown in Table 1. Interestingly, we found that the aggregate  $V_p$  and  $V_s$  values in our study are 5.2% and 8.8% higher, respectively, than those determined by Mashino et al. (2016) using polycrystalline  $\delta$ -AIOOH. Previous studies have shown that the grain size of the polycrystalline aggregate sample and volumetric fraction of grain boundaries significantly affect the obtained velocity in the Brillouin scattering measurements of MgO (Gleason et al. 2011; Marquardt et al. 2011). For example, Gleason et al. (2011) reported that the derived sound wave velocities of MgO powder compressed under nonhydrostatic conditions were lower than those of single-crystal MgO compressed under quasi-hydrostatic conditions. They proposed that the anomalously low velocities were related to the volume fraction of grain boundaries produced by crushed samples under nonhydrostatic conditions. Mashino et al. (2016) used fine-grained polycrystalline  $\delta$ -AIOOH in their Brillouin measurements under ambient conditions. Based on the difference in experimental conditions, the discrepancy between our results and those of Mashino et al. (2016) can be contributed to the grain size and grain boundary effects in the polycrystalline samples. Future systematic studies are needed to clarify this issue.

## IMPLICATIONS

The combination of seismic observations of the deep mantle and elastic results of water-bearing or hydrous minerals can be an effective means to elucidate the water storage, distribution, and circulation in the Earth's interior. We compiled the density, aggregate elastic moduli, aggregate acoustic velocities and anisotropy factors of typical mantle minerals in subducted slabs, and compare them with those of phase Egg and  $\delta$ -AIOOH under ambient conditions (Online Materials<sup>1</sup> Table OM2). The  $AV_p$  and  $AV_s$  values of phase Egg are higher than those of most other minerals, such as olivine, diopside, and wadsleyite; hence, phase Egg is likely a candidate mineral for seismic anisotropy in subducting slabs. The acoustic velocities ( $V_p$  and  $V_s$ ) of phase Egg are remarkably higher than those of the major minerals in the upper mantle (olivine, enstatite, diopside, and majorite) but comparable with those of the minerals

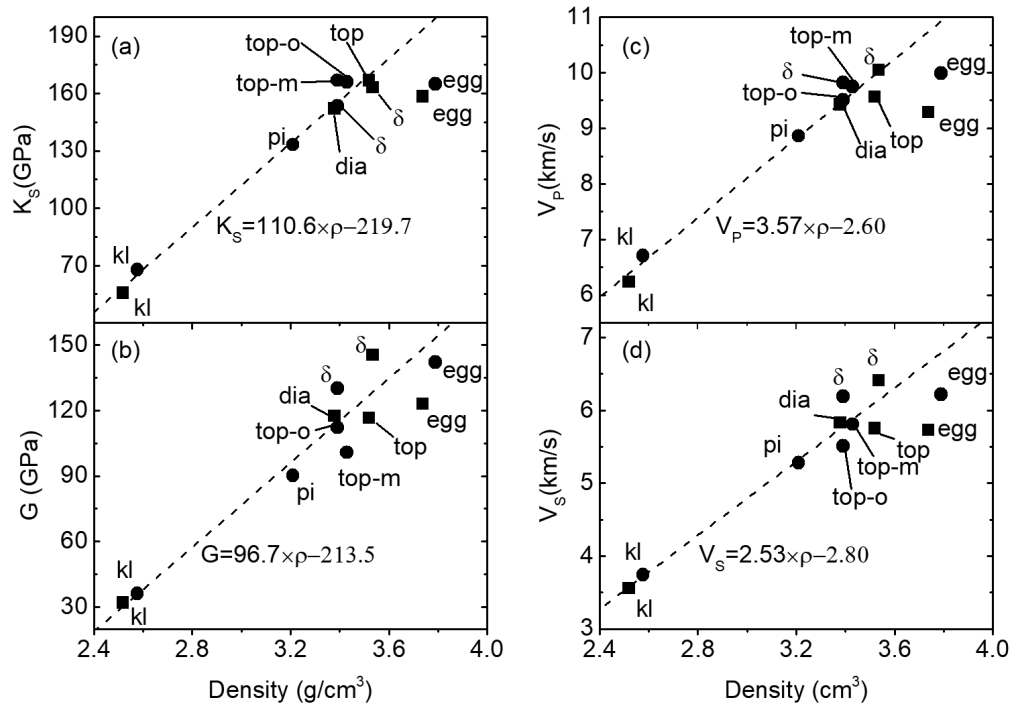


**FIGURE 4.** Elastic moduli and sound velocities of hydrous minerals in the  $\text{Al}_2\text{O}_3$ - $\text{H}_2\text{O}$ - $\text{SiO}_2$  ternary system at ambient conditions. These minerals include kl = kaolinite (Katahara 1996; Scholtzová and Tunega 2020), dia = diaspore (Jiang et al. 2008), pi = phase Pi (Peng et al. 2017), top = topaz (Mookherjee et al. 2016; Tennakoon et al. 2018),  $\delta$  =  $\delta$ - $\text{AlOOH}$  (Tsuchiya and Tsuchiya 2009; this study) and egg = phase Egg (Mookherjee et al. 2019; this study). (a and b) Adiabatic bulk moduli and shear moduli. (c and d) Compressional wave velocities and shear wave velocities. The square and circle symbols represent experimental data and theoretical data, respectively. The dashed lines are linear fitting results of all the data with the exception of phase Egg and the formulas are shown near the lines.

in the mantle transition zone (wadsleyite and ringwoodite). The acoustic velocities of  $\delta$ - $\text{AlOOH}$  are faster than those of all the minerals in the mantle transition zone and the upper mantle but slower than those of the major lower-mantle mineral bridgmanite. Thus, phase Egg may result in a high-velocity anomaly at the depth of the base of the upper mantle, while  $\delta$ - $\text{AlOOH}$  may result in a high-velocity anomaly at the depth of the mantle transition zone. As mentioned before, phase Egg decomposes to  $\delta$ - $\text{AlOOH}$  and stishovite through the  $\text{AlSi}_3\text{OH} = \delta$ - $\text{AlOOH} + \text{SiO}_2$  reaction at relevant  $P$ - $T$  conditions of the topmost lower mantle along the slab geotherm. Based on the elastic data obtained under ambient conditions in this study, the velocity contrast of this reaction is determined to be  $\sim 17\%$  for  $V_p$  and  $\sim 18\%$  for  $V_s$ , which is likely detectable by regional high-resolution seismic tomography. We note that the discussion above is based on elastic data obtained under ambient conditions and the effects of pressure and temperature on the elasticity of these phases are not taken into account. As hydrogen-bond configurations and pressure-induced hydrogen-bond evolution have profound effects on the elastic properties of phase Egg and  $\delta$ - $\text{AlOOH}$  (Mookherjee et al. 2019; Tsuchiya and Tsuchiya 2009), future high-pressure experimental investigations on the elasticity of these two phases are thus critically needed.

To systematically understand the elastic properties of hydrous minerals in the sedimentary layer of subducted slabs, we have plotted the  $K_s$ ,  $G$ ,  $V_p$ , and  $V_s$  of hydrous minerals in the  $\text{Al}_2\text{O}_3$ - $\text{SiO}_2$ - $\text{H}_2\text{O}$  ternary system as a function of density (Fig. 4). The

$K_s$ ,  $G$ ,  $V_p$ , and  $V_s$  values of these hydrous minerals, including kaolinite, phase  $\pi$ , diaspore, topaz, and  $\delta$ - $\text{AlOOH}$ , exhibit a positive linear relationship with the density. Such linear relationships are also observed for the phases along the forsterite-brucite join of the  $\text{MgO}$ - $\text{SiO}_2$ - $\text{H}_2\text{O}$  ternary system. However, the  $K_s$ ,  $G$ ,  $V_p$ , and  $V_s$  values of phase Egg significantly deviate from the linear relationships, showing anomalous elastic behavior probably due to hydrogen-bond configurations in its crystal structure.

#### ACKNOWLEDGMENTS

We thank Vincent Lynch at University of Texas X-ray Diffraction Lab for measuring the crystallographic orientations of the phase Egg.

#### FUNDING

This research at Guangzhou Institute of Geochemistry is financially supported by the Strategic Priority Research Program (B) of the Chinese Academy of Sciences (Grant No. XDB18000000) and the National Natural Science Foundation of China (Grant No. 41874107 and 41574079). J.F.L. acknowledges support from the Geophysics Program of the National Science Foundation, U.S. (EAR-1916941 and EAR-2001381). The single-crystal X-ray diffraction measurements of  $\delta$ - $\text{AlOOH}$  were performed at GSECARS, Advanced Photon Source, Argonne National Laboratory. GSECARS is supported by the National Science Foundation-Earth Sciences (EAR-1634415) and Department of Energy-GeoSciences (DEFG02-94ER14466). This is Contribution No. IS-3099 from GIGCAS.

#### REFERENCES CITED

Dera, P., Zhuravlev, K., Prakapenka, V., Rivers, M.L., Finkelstein, G.J., Grubor-Urosevic, O., Tschauer, O., Clark, S.M., and Downs, R.T. (2013) High pressure single-crystal micro X-ray diffraction analysis with GSE\_ADA/

